Cramer Rao Bound on Target Localization Estimation in MIMO Radar Systems

Hana Godrich°, Alexander M. Haimovich°, and Rick S. Blum†
°New Jersey Institute of Technology, Newark, NJ 07102
†Lehigh University, Bethlehem, PA 18015-3084
°[hg44,haimovich]@njit.edu, †rblum@eecs.lehigh.edu

***Abstract*— This paper presents an analysis of target localization accuracy, attainable by the use of MIMO (Multiple-Input Multiple-Output) radar systems, configured with multiple transmit and receive antennas, widely distributed over a given area. The Cramer-Rao lower bound (CRLB) for target localization is developed for coherent processing. It is shown that the localization estimation accuracy can be approximated as inversely proportional to the carrier frequency in the coherent case. Evaluation of the relation between sensors locations, target location, and localization accuracy is provided by a metric known as geometric dilution of precision (GDOP). GDOP contours map the relative performance accuracy for a given layout of radars over a given geographic area.**

***Index Terms*— MIMO radars, CRLB, target localization.**

I. Introduction

MIMO systems have led to a revolution in wireless communications [1]. Recent publications ([2] and other references therein) indicate that one can exploit similar ideas in radar. MIMO radar is defined broadly as a radar system employing multiple transmit waveforms and having the ability to jointly process signals received at multiple receive antennas. Elements of MIMO radar transmit independent waveforms resulting in an omnidirectional beampattern or create diverse beampatterns by controlling correlations among transmitted waveforms [3]. MIMO radar may be configured with its antennas co-located or widely distributed over an area. In [4] it is observed that MIMO radar has more degrees of freedom than systems with a single transmit antenna. These additional degrees of freedom support flexible time-energy management modes [5], lead to improved angular resolution [6], [7], and support, among other things, high resolution target location [8].

In radar systems, bandwidth plays an important role in determining range resolution, i.e. it is inversely proportional to the signal bandwidth [9] . By exploiting the spatial dimension, coherent MIMO radar with widely separated antennas may overcome bandwidth limitations and support high resolution target localization. The distinction between non-coherent and coherent applications relies on the need for merely time synchronization between the transmitting and receiving radars vs. the need for phase synchronization. The MIMO radar architecture with coherent processing exploits knowledge of the phase differences measured at the receive antennas to produce a high accuracy target location estimate.

The ambiguity function concept has long been used in the context of localization [10]. In [8] it has been used to provide a comparative performance of coherent vs. non-coherent processing of MIMO radar waveforms. The high accuracy localization benefits of coherent MIMO radar systems are inherent in the ambiguity function plots. As the potential for localization performance enhancement is evident from the ambiguity function, the lower bound on the attainable accuracy needs to be evaluated.

In this paper, we explore the performances of coherent MIMO radar target localization. The lower bound on the attainable accuracy is set by developing the Cramer-Rao lower bound (CRLB). The bound is shown to be inversely proportional to the carrier wavelength, and for narrowband signals, independent of the signal bandwidth. The CRLB also provides an insight into the relation between sensors locations, target location, and localization accuracy. To establish a more comprehensive expression of these relations, a metric widely used in Global Positioning Systems (GPS) for mapping estimation precision and known as geometric dilution of precision (GDOP) [11], [12] is introduced. The GDOP contour maps offer a clear description of the impact of multiple dispersed collaborating radars on the resulting accuracy.

II. System Model

Assume M transmitting radars and N receiving radars, widely distributed and time and phase synchronized. The receiving radars could be co-located with the transmitting ones or widely separated. The transmitting and receiving radars are located in a two dimensional plane (x, y). Consider a point target located at coordinates $X = (x, y)$ (see Figure 1). The reflectivity of the target is spatially homogeneous and it is modeled by the complex value $\zeta = \zeta_{re} + j\zeta_{im}$. Now, let the target be illuminated by M transmitters arbitrarily located at coordinates $T_k = (x_{tk}, y_{tk})$, $k = 1, \ldots, M$. The signals scattered by the target are collected by N sensors placed at arbitrary coordinates $R_\ell = (x_{r\ell}, y_{r\ell})$, $\ell = 1, \ldots, N$. The set of transmitted waveforms in lowpass equivalent form is $\sqrt{E_e} s_k(t)$, $k = 1, \ldots, M$, where $\int_{\mathcal{T}} |s_k(t)|^2 dt = 1$, $E_e = E/M$ is the normalized transmitted energy (while E is the total transmitted energy), and $\mathcal{T}$ is the waveforms' duration. Let all transmitted waveforms have the same bandwidth W.

A. M. Haimovich work was supported by the U.S. Air Force Office of Scientific Research, Agreement FA9550-06-1-0026. R. S. Blum work was supported by the Air Force Research Laboratory under agreement No. FA9550-06-1-0041

Further specification of the waveforms $s_k(t)$ depends on the application. The transmitted waveforms are orthogonal and we assume that orthogonality is maintained even for different mutual delays, i.e., $\int_{\mathcal{T}} s_k(t)\, s_m^*(t-\tau)\, dt = 0$ for all $k \neq m$, and for all time delays of interest.

In the model developed below, path loss effects are neglected, i.e., the model accounts for the effect of the sensors/target localizations only through time delays (or phase shifts) of the signals. For convenience, we define a four dimensioned vector θ of the unknown parameters:

$$\theta \stackrel{\text{def}}{=} [x, y, \zeta_{re}, \zeta_{im}]^T. \tag{1}$$

The propagation time estimate of a signal transmitted by the k-th transmitting radar located at coordinates $T_k = (x_{tk}, y_{tk})$,reflected by a target located at $X = (x, y)$ and received by a radar located at $R_l = (x_{rl}, y_{rl})$ can be approximated as:

$$\widehat{\tau}_{lk} = \tau_{lk} + \varepsilon_{lk}, \qquad \forall k = 1, .., M, l = 1, .., N, \tag{2}$$

where τ_{lk}, the propagation time, is the sum of the time delays from radar k to the target and from the target to radar l:

$$\tau_{lk} = \frac{\sqrt{(x_{tk}-x)^2 + (y_{tk}-y)^2}}{c} + \frac{\sqrt{(x_{r\ell}-x)^2 + (y_{r\ell}-y)^2}}{c}, \tag{3}$$

and the estimation error ε_{lk} can be shown [13] to have a Gaussian distribution $\mathcal{N}\left(0, \sigma_\epsilon^2\right)$.

Consider the case of a baseband representation of the signal observed at sensor ℓ due to a transmission from sensor k and reflection from a scatterer at coordinates $X = (x, y)$, given by:

$$r_\ell(t) = \sqrt{E_e} \sum_{k=1}^{M} \zeta s_k(t - \tau_{\ell k})\, \rho_{\ell k} + w_\ell(t), \tag{4}$$

where $\rho_{\ell k}$ accounts for the phase information and has the value of $\rho_{\ell k}(c) = \exp(-j2\pi f_c \tau_{\ell k})$. Others terms are the carrier frequency f_c , the speed of light c, and $w_\ell(t)$ is circularly symmetric, zero-mean, complex Gaussian noise, spatially and temporally white with autocorrelation function $\sigma_w^2 \delta(\tau)$. We define the vectors $\mathbf{r} = [r_1(t), \ldots, r_N(t)]^T$ and $\boldsymbol{\psi} = [\tau_{11}, \tau_{12}, ..., \tau_{MN}, \zeta_{re}, \zeta_{im}]^T$ for later use. The received signal at each sensor is a mixture of the transmitted signals reflected by the target. The mixture of signals is separated at the receiver end by exploiting the orthogonality between the transmitted waveforms.

III. The CRLB on On Target Localization Estimation

The CRLB provides a lower bound for the mean square error (MSE) of any unbiased estimator for an unknown parameter(s). Given a vector parameter $\boldsymbol{\theta}$, its unbiased estimate $\widehat{\boldsymbol{\theta}}$ satisfies the following inequality [14]:

$$E_{\boldsymbol{\theta}}\left\{\left(\widehat{\theta}_i - \theta_i\right)\left(\widehat{\theta}_i - \theta_i\right)^T\right\} \geq \left[\mathbf{J}^{-1}(\boldsymbol{\theta})\right]_{i,i} \tag{5}$$

where $\mathbf{J}(\boldsymbol{\theta})$ is the Fisher Information matrix (FIM) given by:

$$\mathbf{J}(\boldsymbol{\theta}) \stackrel{\text{def}}{=} E_{\boldsymbol{\theta}}\left\{\frac{\partial}{\partial \boldsymbol{\theta}} \log p(\mathbf{r}|\boldsymbol{\theta}) \left(\frac{\partial}{\partial \boldsymbol{\theta}} \log p(\mathbf{r}|\boldsymbol{\theta})\right)^T\right\}. \tag{6}$$

where $p(\mathbf{r}|\boldsymbol{\theta})$ is the joint probability density function (pdf) of $\boldsymbol{\theta}$.

Let the CRLB matrix be defined as:

$$\mathbf{C}_{CRLB} = [\mathbf{J}(\boldsymbol{\theta})]^{-1}. \tag{7}$$

Since the received signal in (4) is defined as a function of the time of arrival, $\tau_{\ell k}$, and the reflectivity value $\zeta = \zeta_{re} + j\zeta_{im}$,with the use of the *chain rule*, $\mathbf{J}(\boldsymbol{\theta})$ could be decomposed to an alternative form [14] where the FIM is express as :

$$\mathbf{J}(\boldsymbol{\theta}) = \mathbf{P} \cdot \mathbf{J}(\boldsymbol{\psi}) \cdot \mathbf{P}^T, \tag{8}$$

where:

$$\mathbf{P} = \frac{\partial \boldsymbol{\psi}}{\partial \boldsymbol{\theta}} = \begin{bmatrix} \frac{\partial \tau_{11}}{\partial x} & \ldots & \frac{\partial \tau_{MN}}{\partial x} & \frac{\partial \zeta_{re}}{\partial x} & \frac{\zeta_{im}}{\partial x} \\ \frac{\partial \tau_{11}}{\partial y} & \ldots & \frac{\partial \tau_{MN}}{\partial y} & \frac{\partial \zeta_{re}}{\partial y} & \frac{\zeta_{im}}{\partial y} \\ \frac{\partial \tau_{11}}{\partial \zeta_{re}} & \ldots & \frac{\partial \tau_{MN}}{\partial \zeta_{re}} & \frac{\partial \zeta_{re}}{\partial \zeta_{re}} & \frac{\zeta_{im}}{\partial \zeta_{re}} \\ \frac{\partial \tau_{11}}{\partial \zeta_{im}} & \ldots & \frac{\partial \tau_{MN}}{\partial \zeta_{im}} & \frac{\partial \zeta_{re}}{\partial \zeta_{im}} & \frac{\zeta_{im}}{\partial \zeta_{im}} \end{bmatrix}, \tag{9}$$

is an $4\text{x}(MN+2)$ matrix, and $\mathbf{J}(\boldsymbol{\psi})$ is the FIM for the unknown vector $\boldsymbol{\psi}$:

$$\mathbf{J}(\boldsymbol{\psi}) = E_{\boldsymbol{\psi}}\left\{\frac{\partial}{\partial \boldsymbol{\psi}} \log p(\mathbf{r}|\boldsymbol{\psi}) \left(\frac{\partial}{\partial \boldsymbol{\psi}} \log p(\mathbf{r}|\boldsymbol{\psi})\right)^T\right\}. \tag{10}$$

Matrix $\mathbf{P}$ is derived using the relation given in (3) and is of the form:

$$\mathbf{P} = -\frac{1}{c} \begin{bmatrix} \mathbf{H}_{MN\text{x}MN} & \mathbf{0}_{MN\text{x}2} \\ \mathbf{0}_{2\text{x}MN} & \mathbf{I}_{2\text{x}2} \end{bmatrix}, \tag{11}$$

where $\mathbf{H}$ is defined as:

$$\mathbf{H} = \begin{bmatrix} A_{11} & \ldots & A_{MN} \\ B_{11} & \ldots & B_{MN} \end{bmatrix}_{MN\text{x}MN}, \tag{12}$$

using the notation $A_{\ell k} = \cos\phi_{tk} + \cos\phi_{r\ell}$ and $B_{\ell k} = \sin\phi_{tk} + \sin\phi_{r\ell}$, where the phase elements are $\phi_{tk} = \tan^{-1}\left(\frac{y-y_{tk}}{x-x_{tk}}\right)$ and $\phi_{rl} = \tan^{-1}\left(\frac{y-y_{rl}}{x-x_{rl}}\right)$. Matrix $\mathbf{H}$ includes the geometric information of the radars location configuration relative to the target position.

A. CRLB and the minimum mean-square error (MMSE):

Given a set of known waveforms $s_k\left(t-\tau_{\ell k}\right)$ parameterized by the unknown time delays $\tau_{\ell k}$, which in turn are a function of the unknown target location $X=(x,y)$, for the signal model (4), the joint pdf of the observations (time samples at multiple receive antennas) parameterized by the unknown parameters vector $\boldsymbol{\psi}$, is then:

$$p_c\left(\mathbf{r}|\boldsymbol{\psi}\right) \propto \exp \tag{13}$$
$$\left\{-\frac{1}{\sigma_w^2}\sum_{\ell=1}^{N}\int_T\left|r_\ell(t)-\sqrt{E_e}\sum_{k=1}^{M}\zeta s_k\left(t-\tau_{\ell k}\right)\rho_{\ell k}\right|^2 dt\right\}$$

Deriving the elements of $\mathbf{J}_c\left(\boldsymbol{\psi}\right)$, using (13) provides the following results:

$$\mathbf{J}_c(\boldsymbol{\psi})=\left[\begin{array}{cc}\boldsymbol{\Lambda}_{\mathbf{x}c} & \mathbf{V}\\ \mathbf{V}^T & \boldsymbol{\Lambda}_\zeta\end{array}\right]_{(MN+2)\mathrm{x}(MN+2)}, \tag{14}$$

where we use the following notation for $\boldsymbol{\Lambda}_{\mathbf{x}c}$:

$$\begin{aligned}\boldsymbol{\Lambda}_{\mathbf{x}c} &= 8\pi^2 SNR\left(f_c^2+\beta^2\right)\mathbf{I}_{NM\times NM}, \qquad (15)\\ \boldsymbol{\Lambda}_\zeta &= SNR\frac{MN}{|\zeta|^2}\mathbf{I}_{2\times 2},\\ \mathbf{V} &= \frac{4\pi f_c SNR}{|\zeta|^2}\left[\begin{array}{cc}-\zeta_{im} & \zeta_{re}\\ \vdots & \vdots\\ -\zeta_{im} & \zeta_{re}\end{array}\right]_{NM\times 2},\end{aligned}$$

where we define the signal-to-noise ratio as $SNR=\frac{\left|\sqrt{E_e}\zeta\right|^2}{\sigma_w^2}$. The term β is the effective bandwidth defined as $\beta^2=\frac{\int_W f^2|S(f)|^2df}{\int_W|S(f)|^2df}$, where the integration is over the bandwidth W.

In order to determine the value of $\mathbf{J}_c\left(\boldsymbol{\theta}\right)$ for the coherent case we use (14) and (11) in (8) to get:

$$\mathbf{J}_c\left(\boldsymbol{\theta}\right)=\frac{1}{c^2}\left[\begin{array}{cc}\mathbf{H}\boldsymbol{\Lambda}_{\mathbf{x}c}\mathbf{H}^T & \mathbf{V}\mathbf{H}\\ \mathbf{H}^T\mathbf{V}^T & \boldsymbol{\Lambda}_\zeta\end{array}\right]. \tag{16}$$

While the CRLB expresses the lower bound on the mean-square error (MSE) of the estimate of $\boldsymbol{\theta}=[x,y,\zeta_{re},\zeta_{im}]^T$, we are really interested only in the estimation of x and y. The target reflectivity terms ζ_{re} and ζ_{im} serve as nuisance parameters. For the variances of the estimates of x and y, it is sufficient to derive the submatrix $[\mathbf{C}_{CRLB_c}]_{2\times 2}=[\mathbf{J}_c\left(\boldsymbol{\theta}\right)]^{-1}_{2\times 2}$, denoting the first 2x2 submatrix of $[\mathbf{J}_c\left(\boldsymbol{\theta}\right)]^{-1}$.

Proposition 1: The CRLB submatrix for the target position estimates for the coherent case is:

$$[\mathbf{C}_{CRLB_c}]_{2\mathrm{x}2}=\left(\mathbf{H}\boldsymbol{\Lambda}_{\mathbf{x}c}\mathbf{H}^T-\mathbf{V}\mathbf{H}\boldsymbol{\Lambda}_\zeta^{-1}\mathbf{H}^T\mathbf{V}^T\right)^{-1}, \tag{17}$$

The MMSE for the target position for the x axis is

$$\sigma^2_{x_cMMSE}=\frac{c^2}{8\pi^2 SNR f_c^2\left(1+\frac{\beta^2}{f_c^2}\right)}\cdot\frac{g_{xc}}{u_{CRLB_c}} \tag{18}$$

and for the y axis is

$$\sigma^2_{y_cMMSE}=\frac{c^2}{8\pi^2 SNR f_c^2\left(1+\frac{\beta^2}{f_c^2}\right)}\cdot\frac{g_{yc}}{u_{CRLB_c}} \tag{19}$$

where the terms u_{CRLB_c}, g_{xc} and g_{yc} relate to the geometric layout of the transmitting and receiving radars compared with the target location and the ratio term $f_R=\left(1+\frac{\beta^2}{f_c^2}\right)$.

Proof: see Appendix A for proof of (17). The $\mathbf{C}_{CRLB_c2\mathrm{x}2}$ submatrix provides the information for $\sigma^2_{x_c}\geq[\mathbf{C}_{CRLB_c}]_{1,1}$ and $\sigma^2_{y_c}\geq[\mathbf{C}_{CRLB_c}]_{2,2}$. The MMSEs are obtained by using (15) in (17), where we get (18) and (19) with the following value for the x axis coefficient g_{xc} :

$$g_{xc}=\left[sum\left(B_{\ell k}^2\right)-\frac{\left(sum\left(B_{\ell k}\right)\right)^2}{f_RMN}\right], \tag{20}$$

where the following notation is used $sum\left(\circ\right)=\sum_{k=1}^{M}\sum_{\ell=1}^{N}\left(\circ\right)$. The y axis coefficient g_{yc} :

$$g_{yc}=\left[sum\left(A_{\ell k}^2\right)-\frac{\left(sum\left(A_{\ell k}\right)\right)^2}{f_RMN}\right], \tag{21}$$

and the common term u_{CRLB_c} is:

$$\begin{aligned}u_{CRLB_c} &= [g_{xc}]\cdot[g_{yc}] \qquad (22)\\ &\quad -\left[sum\left(A_{\ell k}B_{\ell k}\right)-\frac{sum\left(A_{\ell k}\right)sum\left(B_{\ell k}\right)}{f_RMN}\right]^2.\end{aligned}$$

These terms are summations of the terms $A_{\ell k}$ and $B_{\ell k}$ that represent sine and cosine of the angles ϕ_{tk} and ϕ_{rl} and therefore, the geometric relation between the sensors locations and the target location.It is apparent that for the coherent case the MMSEs for the target location estimates in (18) and (19) are inversly proportional to the ratio term f_R and to the carrier frequency f_c^2. ■

B. Discussion

Now that the expressions for the MMSEs for target location estimate has been derived, we can provide some interpretations:

• The MMSEs expressions show that the achievable accuracy is inversely proportional to $f_c^2(1+\frac{\beta^2}{f_c^2})$, due to the use of the phase information across different paths. For narrow band signals, where $\frac{\beta}{f_c}\ll 1$, and therefore, $f_R\approx 1$, the localization accuracy is inversely proportional to the carrier frequency f_c^2 and independent of the effective bandwidth. It is apparent that coherent processing offers an accuracy gain when compared with the effective bandwidth, for narrow band signals.

• The MMSEs terms are strongly reliant on the geographical spread of the radar systems, compared with the target location. This dependency is integrated into the terms $\frac{g_{xc}}{u_{CRLB_c}}$ and $\frac{g_{yc}}{u_{CRLB_c}}$. From these terms one cannot intuitively identify the relation between the radars positions and the obtainable accuracy. For this reason, we need to define a more suitable method to express these relations. The GDOP metric, introduced in the next section, provides these tools.

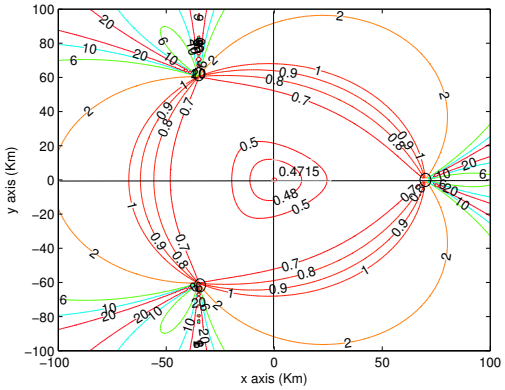

Fig. 1. GDOP map for a symmetric positioning of radars around the axis origin: case (a) for M=N=3.

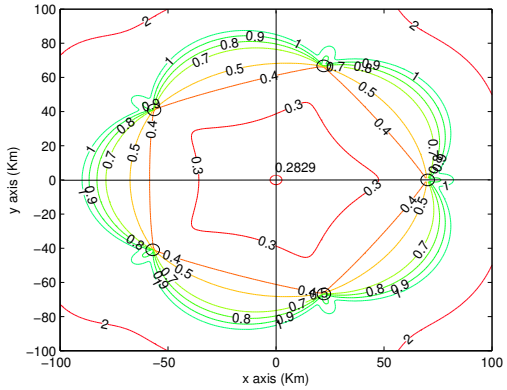

Fig. 2. GDOP contours for a symmetric positioning of radars around the axis origin: case (b) for M=N=5.

• The CRLB is known to provide a good bound in high SNR. As for low SNR, the CRLB does not give a rigorous bound. As the time estimates are based on matched filters at the receiver end, the ambiguity features of the signal waveforms predominate the estimation capabilities in low SNR conditions. A more rigid bound needs to be found for the localization error variance in the low SNR case.

IV. GDOP

The GDOP metric is commonly used in GPS for mapping the attainable localization precision for a given layout of GPS satellites positions [11], [12]. Here, we seek a metric that expresses the effect of the positions of the transmitting and receiving elements of the MIMO radar on the relationship between the time delay estimation errors and the localization errors.

The GDOP metric for the two dimensional case is defined:

$$\text{GDOP} = \frac{\sqrt{\sigma_x^2 + \sigma_y^2}}{c\sigma_\epsilon}, \tag{23}$$

where σ_x^2 and σ_y^2 are the variances of localization on the x and y axis, respectively, and σ_ϵ is the standard deviation of the time delays, assumed the same for all sensors. Inherently, this metric provides a normalized value that represents the relative contribution of the radars' location to the overall accuracy. Substituting σ_x^2 and σ_y^2 by the coherent MMSE given in (18) and (19), and using the result in [13] for the time delay variance, we get the following GDOP expression:

$$\text{GDOP}_c = \sqrt{\frac{g_{xc} + g_{yc}}{u_{CRLB_c}}}. \tag{24}$$

In this expression, the sensors' locations are embedded in the terms $A_{\ell k}$ and $B_{\ell k}$. The GDOP reduces the combined effect of the locations to a single metric. Once we get the values mapped, the actual localization error is easily derived by multiplying the GDOP value with $c\sigma_\epsilon$.

In Figures 1 and 2, contour plots of the GDOP values are presented for the case of respectively, $M = N = 3$ and $M = N = 5$ radars positioned symmetrically on the N vertices of a polygon centered at the origin. The radars are all transmitting orthogonal signals and perform time delay estimations. The first noticeable factor in the comparison of the two plots is the higher accuracy obtained with five radars compared to three radars. For example, the lowest GDOP value for the case of three radars is 0.4715, while with five radars, the GDOP is 0.2829, corresponding to a 60% improvement. All the targets located inside the virtual N-sided polygon achieve relative high accuracy localization, while the most accurate localization is obtained for the target at the center. The increase in GDOP values from the center to the polygon boundaries is slow. Outside this polygon, the GDOP values increase rather rapidly.

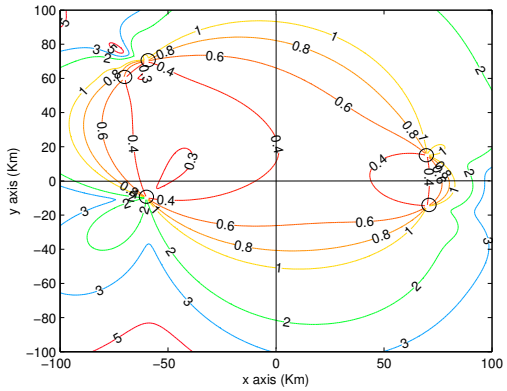

Fig. 3. GDOP contours for an asymmetric positioning of radars around the axis origin.

In Figures 3 and 4 contours of five non-symmetrically positioned radars are drawn. When the radars are spread around the target (Figure 3), there are still some areas with good measurement accuracy, though the coverage is shrunk compared to the case with symmetrical distribution of sensors in Figure 2. When the viewing angle of the target is very restricted, as in the bottom of Figure 4, there is a marked

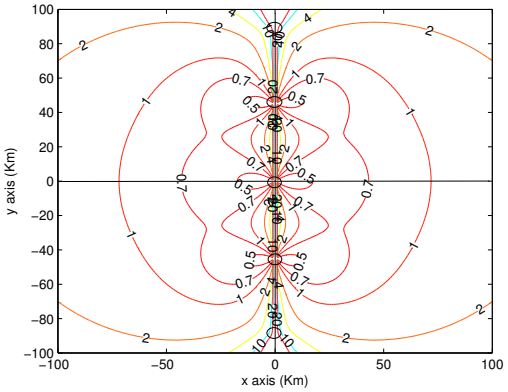

Fig. 4. GDOP contours for the case where the radar are aligned.

degradation of GDOP values.

These examples have shown that a symmetrical deployment of sensors around the target yield lowest GDOP values. They bring up the question what is the lowest GDOP that can be obtained.

A. Lowest GDOP

Theoretical analysis of the lowest attainable GDOP for a passive system (such as GPS) was performed in [12]. It shows that for a system with N satellites optimally positioned around the user, where the user measures the signals' time of arrival to estimate its position, the lowest achievable GDOP value is $2/\sqrt{N}$. It is shown in Appendix B that for a MIMO radar system with M transmitters and N receivers, the lowest achievable GDOP can be approximate by $\sqrt{2/MN}$, where for $M = N$ it is equal to $\sqrt{2/N^2}$. This result is interpreted as a "MIMO advantage" compared to the single transmit antennas case. As a numerical example, the lowest GDOPs in Figures 1 and 2 are $\sqrt{2/3^2} \simeq 0.4715$ and $\sqrt{2/5^2} \simeq 0.2829$ respectively.

V. Conclusions

We have developed analytical expressions for the estimation errors of coherent MIMO radar using the CRLB. It discloses the accuracy dependence on the carrier wavelength, and its independence on the effective bandwidth for narrow band signals, showing the coherent MIMO radar system advantage in locating targets with high resolution. The effect of the geometry of the sensors is also captured. Plots of GDOP provide a clear view of high accuracy areas for a given set of radar locations. These plots could also serve as a tool for choosing favorable radar locations to cover a given target area. As the coherent systems provide significantly better performance, at the same time, this type of MIMO radar has the challenge of time and/or phase synchronizing multisite systems, and needs to deal with ambiguities stemming from the large separation between sensors.

.

Appendix

A: Proof of Proposition 1

The submatrix $[\mathbf{C}_{CRLB}]_{2\text{x}2}$ is defined as:

$$[\mathbf{C}_{CRLB_c}]_{2\text{x}2} = [\mathbf{J}_c(\boldsymbol{\theta})]^{-1}_{2\text{x}2}. \tag{25}$$

For a given matrix of the form:

$$\mathbf{J}_c(\boldsymbol{\theta}) = \begin{bmatrix} \mathbf{H}\boldsymbol{\Lambda}_{\mathbf{x}c}\mathbf{H}^T_{NM\text{x}NM} & \mathbf{V}\mathbf{H}_{NM\text{x}2} \\ \mathbf{H}^T\mathbf{V}^T_{2\text{x}NM} & \boldsymbol{\Lambda}_{\zeta_{2\text{x}2}} \end{bmatrix}, \tag{26}$$

where $\boldsymbol{\Lambda}_\zeta$ is a diagonal matrix of the form $\boldsymbol{\Lambda}_\zeta = d\mathbf{I}_{2\times 2}$, and d is some constant.

By definition, the value of $[\mathbf{J}_c(\boldsymbol{\theta})]^{-1}_{1,1}$ is obtained by:

$$[\mathbf{J}_c(\boldsymbol{\theta})]^{-1}_{1,1} = \frac{\left|\widetilde{\mathbf{J}_c}(\boldsymbol{\theta})_{ex(1,1)}\right|}{|\mathbf{J}_c(\boldsymbol{\theta})|}, \tag{27}$$

where $|\cdot|$ denotes the determinant, and $\widetilde{\mathbf{J}_c}(\boldsymbol{\theta})_{ex(1,1)}$ is an $(NM+1)\times(NM+1)$ matrix, obtained by removing the first row and the first column of the $\mathbf{J}_c(\boldsymbol{\theta})$ matrix. The determinant of $\mathbf{J}_c(\boldsymbol{\theta})$, using the property that the determinant of a matrix does not change under linear operations, is:

$$|\mathbf{J}_c(\boldsymbol{\theta})| = \begin{vmatrix} \mathbf{H}\boldsymbol{\Lambda}_{\mathbf{x}c}\mathbf{H}^T - \mathbf{V}\mathbf{H}\boldsymbol{\Lambda}_\zeta^{-1}\mathbf{H}^T\mathbf{V}^T & \mathbf{0} \\ \mathbf{H}^T\mathbf{V}^T & \boldsymbol{\Lambda}_\zeta \end{vmatrix}. \tag{28}$$

This can be calculated and expressed as:

$$|\mathbf{J}_c(\boldsymbol{\theta})| = \left|\mathbf{H}\boldsymbol{\Lambda}_{\mathbf{x}c}\mathbf{H}^T - \mathbf{V}\mathbf{H}\boldsymbol{\Lambda}_\zeta^{-1}\mathbf{H}^T\mathbf{V}^T\right| |\boldsymbol{\Lambda}_\zeta|. \tag{29}$$

Repeating the same for the matrix $\widetilde{\mathbf{J}_c}(\boldsymbol{\theta})_{ex(1,1)}$:

$$\widetilde{\mathbf{J}_c}(\boldsymbol{\theta})_{ex(1,1)} = \begin{bmatrix} \widetilde{\mathbf{H}\boldsymbol{\Lambda}_{\mathbf{x}c}\mathbf{H}^T}_{ex(1,1)} & \widetilde{\mathbf{V}\mathbf{H}}_{ex(1,)_{NM-1\text{x}2}} \\ \widetilde{\mathbf{H}^T\mathbf{V}^T}_{ex(,1)_{2\text{x}NM-1}} & \boldsymbol{\Lambda}_\zeta \end{bmatrix}. \tag{30}$$

Using the same matrix manipulation, we get:

$$\left|\widetilde{\mathbf{J}}(\boldsymbol{\theta})_{ex(1,1)}\right| = \left|\widetilde{\mathbf{H}\boldsymbol{\Lambda}_{\mathbf{x}c}\mathbf{H}^T} - \widetilde{\mathbf{V}\mathbf{H}}\boldsymbol{\Lambda}_\zeta^{-1}\widetilde{\mathbf{H}^T\mathbf{V}^T}\right| |\boldsymbol{\Lambda}_\zeta|, \tag{31}$$

and using terms (29) and (31) in (27) yields:

$$[\mathbf{J}_c(\boldsymbol{\theta})]^{-1}_{1,1} = \frac{\left|\widetilde{\mathbf{H}\boldsymbol{\Lambda}_{\mathbf{x}c}\mathbf{H}^T} - \widetilde{\mathbf{V}\mathbf{H}}\boldsymbol{\Lambda}_\zeta^{-1}\widetilde{\mathbf{H}^T\mathbf{V}^T}\right|}{\left|\mathbf{H}\boldsymbol{\Lambda}_{\mathbf{x}c}\mathbf{H}^T - \mathbf{V}\mathbf{H}\boldsymbol{\Lambda}_\zeta^{-1}\mathbf{H}^T\mathbf{V}^T\right|}. \tag{32}$$

By definition, this expression is identical to:

$$[\mathbf{J}_c(\boldsymbol{\theta})]^{-1}_{1,1} = \left[\left(\mathbf{H}\boldsymbol{\Lambda}_{\mathbf{x}c}\mathbf{H}^T - \mathbf{V}\mathbf{H}\boldsymbol{\Lambda}_\zeta^{-1}\mathbf{H}^T\mathbf{V}^T\right)^{-1}\right]_{1,1}. \tag{33}$$

Repeating the process for term located at $(1,2)$, $(2,1)$, and $(2,2)$, results in:

$$[\mathbf{C}_{CRLB_c}]_{2\times 2} = \left(\mathbf{H}\boldsymbol{\Lambda}_{\mathbf{x}c}\mathbf{H}^T - \mathbf{V}\mathbf{H}\boldsymbol{\Lambda}_\zeta^{-1}\mathbf{H}^T\mathbf{V}^T\right)^{-1}. \tag{34}$$

.

APPENDIX

B: Deriving the lowest GDOP

Using the expression for the GDOP in (24), and the definitions of terms $A_{\ell k}$, $B_{\ell k}$ for (12), we analyze the following special scenario: assume N radars are located symmetrically on the corners of an N-sided regular polygon centered at the origin, where $N \geq 3$. The target is located at the axis origin $X_0 = (0,0)$. The angles between the radars and the target for this case are: $\phi_{tk} = \frac{2\pi(k-1)}{N}$ and $\phi_{rl} = \frac{2\pi(l-1)}{N}$. For this case, the following Fourier summation formulas apply:

$$\sum_{k=1}^{N} \cos^2 \frac{2\pi\,(k-1)}{M} = \sum_{k=1}^{N} \sin^2 \frac{2\pi\,(k-1)}{M} = \frac{N}{2}, \qquad (35)$$

and;

$$\sum_{k=1}^{N} \cos \frac{2\pi\,(k-1)}{N} \sin \frac{2\pi\,(k-1)}{N} = 0. \qquad (36)$$

Case (a): for an $N \times N$ system: using the Fourier summation formulas, we get

$$sum\left(A^2\right) = sum\left(B^2\right) = N^2, \qquad (37)$$

and;

$$sum(A) = sum(B) = sum(AB) = 0,$$

This results in

$$GDOP_{NxN} = \sqrt{\frac{2}{N^2}}. \qquad (38)$$

Case (b): for an $M \times N$ system: all N radars are receiving the signal waveforms transmitted by M radars, where $1 < M < N$. Using the same mechanism as done previously, neglectingand sine and cosine terms in the power of two and more, we get:

$$GDOP_{MxN} \approx \sqrt{\frac{2}{NM}}. \qquad (39)$$

REFERENCES

[1] G. J. Foschini, "Layered space-time architecture for wireless communication in a fading environment when using multiple antennas," *Bell Labs Technical Journal*, vol. 1, no. 2, pp. 41-59, 1996.

[2] E. Fishler, A. Haimovich, R. Blum, L. Cimini, D. Chizhik, and R. Valenzuela, "Spatial diversity in radars - models and detection performance," *IEEE Trans. on Sig. Proc.*, vol. 54, March 2006, pp. 823-838.

[3] D. R. Fuhrman, and G. San Antonio, "Transmit beam-forming for MIMO radar systems using partial signal correlation," in *Proc. of 38th ASILOMAR 2004 Conf. on Signals, Systems and Computers,* Nov. 2004, pp. 295–299.

[4] D. W. Bliss and K. W. Forsythe, "Multiple-input multiple-output (MIMO) radar and imaging: degrees of freedom and resolution," in *Proc. of 37th Asilomar Conference on Signals, Systems and Computers,* Nov. 2003, pp. 54-59.

[5] D. Rabideau, "Ubiquitous MIMO digital array radar," in *Proc. of 37th Asilomar Conf. on Signals, Systems, and Computers*, Nov. 2003, pp. 1057-1064.

[6] F. C. Robey, S. Coutts, D. Weikle, J. C. McHarg, and K. Cuomo, "MIMO radar theory and experimental results," in the *38th Asilomar Conference on Signals, Systems and Computers*, November 2004, pp. 300–304.

[7] I. Bekkerman and J. Tabrikian, "Target detection and localization using MIMO radars and sonars," *IEEE Trans. on Sig. Proc.*, vol. 54, Oct. 2006, pp. 3873- 3883.

[8] N.H. Lehmann, A.M Haimovich , R.S. Blum, L.J.Cimini, "High Resolution Capabilities of MIMO Radar," in *Proc. of 40th Asilomar Conf. on Signals, Systems and Computers,* Nov. 2006.

[9] M. Skolnik, *Introduction to Radar Systems*, 3rd ed., New York: McGraw-Hill, 2002.

[10] N. Levanon, *Radar Principles,* New York: John Wiley and Sons Inc, 1st ed., 1988.

[11] H. B. Lee, "A novel procedure for assessing the accuracy of the hyperbolic multilateration systems," *IEEE Trans. on Aerospace and Electronic Systems*, vol. 11, pp. 2-15, Jan. 1975.

[12] N. Levanon, "Lowest GDOP in 2-D scenarios," *IEE Proc.-Radar, Sonar, Navig.*, vol. 147, pp. 149-155, June 2000.

[13] H. Godrich, A.M Haimovich, and R.S. Blum, "*Concepts And Applications Of MIMO Radar Sysem With Widely Separated Antenna.,*" Book Chapter, in preparation, 2007.

[14] S. M. Kay, *Fundementals of Statistical Signal Processing: Estimation Theory,* vol. 1, New Jersey: Parentice Hall PTR, 1st ed., 1993.